Aerosol optical depth retrieval from GOES-8: Uncertainty study and retrieval validation over South America

Kenneth R. Knapp[1] and Thomas H. Vonder Haar

Cooperative Institute for Research in the Atmosphere and Department of Atmospheric Science, Colorado State University, Fort Collins, Colorado, USA

Yoram J. Kaufman

NASA Goddard Space Flight Center, Greenbelt, Maryland, USA

Received 21 February 2001; revised 3 August 2001; accepted 20 August 2001; published 11 April 2002.

[1] An algorithm for aerosol optical depth τ retrieval from the Geostationary Observational Environmental Satellite (GOES) series is described, where the darkest pixels are used to create a spatial composite of surface reflectance. The data are calibrated and corrected for atmospheric extinction to retrieve the surface reflectance which is then used to retrieved τ. Analysis suggests that τ retrieval uncertainty is $\pm 18-34\%$ depending on the certainty of the assumed radiative transfer model parameters. Retrieval uncertainty is less over low surface reflectances and at large scattering angles. The retrieval algorithm is validated against Sun-sky radiometer τ measurements for aerosols emitted by biomass burning in South America during 1995 and 1998. The relative differences between observed and retrieved τ are within the estimated uncertainty, having correlations ranging from 0.78 to 0.97. Further, the GOES retrievals are compared to τ retrieved using the Moderate-Resolution Imaging Spectroradiometer (MODIS) airborne simulator (MAS). The average relative difference in this comparison is 11%, thus retrieval validations are again within the estimated algorithm uncertainty. These results suggest that the GOES satellite can be used to monitor aerosols over land, while the agreement between MAS and GOES retrievals suggests the ability to combine the spectral abilities of MODIS with the temporal observations of GOES. *INDEX TERMS:* 1640 Global Change: Remote sensing; 0305 Atmospheric Composition and Structure: Aerosols and particles (0345, 4801); 1694 Global Change: Instruments and techniques; 0394 Atmospheric: Composition and Structure: Instruments and techniques; *KEYWORDS:* aerosol, optical depth, remote sensing, GOES

1. Introduction

[2] The magnitude to which aerosols impact the climate system of the Earth is uncertain [*Hansen et al.*, 2000], so the need for the understanding of the global distribution of aerosols is great. Recent studies have shown that the Moderate-Resolution Spectroradiometer (MODIS) and Multiangle Imaging SpectroRadiometer (MISR) instruments will provide an estimate of their distribution over land and ocean [*Tanré et al.*, 1997; *Kaufman et al.*, 1997; *Diner et al.*, 1996]. Yet these retrievals will be limited in temporal resolution. While aerosols may not exhibit a systematic diurnal trend [*Kaufman et al.*, 2000], the continuous measurement of aerosol optical depth could provide information on aerosol emissions and transport from strong sources (e.g., biomass burning). In this respect, the understanding of aerosols would benefit from accurate measurements of MODIS and MISR as well as the temporal component provided by Geostationary Operational Environmental Satellites (GOES). The goal of this study is to demonstrate the viability of using both geostationary and polar orbiting satellites for climatological studies of the Earth through the development and validation of a GOES aerosol retrieval algorithm. While the instruments launched on the Earth Observation System satellites have specific channels to derive aerosol optical properties, they lack the diurnal observations to fully quantify the aerosol effects. Conversely, GOES can observe the diurnal changes in aerosol properties. By combining the observations of the systems, the advantages of both systems could be utilized.

[3] Qualitative detection of aerosols over land dates back to the first Advanced Technology Satellite (ATS-I) in monitoring of pollution in the Los Angeles area [*Lyons et al.*, 1978]. Since then, quantitative satellite remote sensing of aerosols over land from the visible spectrum has used the following: synchronous meteorological satellite (SMS-I) [*Lyons et al.*, 1978], Thematic Mapper (TM) imagery [*Mekler and Kaufman*, 1980] GOES-1 [*Fraser et al.*, 1984], advanced very high resolution radiometer (AVHRR) [*Kaufman et al.*, 1990; *Soufflet et al.*, 1997], and total ozone mapping spectrometer (TOMS) [*Herman et al.*, 1997a]. These early studies often compare two satellite images to obtain an aerosol estimate: one from a relatively "clear" day with relatively low aerosol burden and a "hazy" day which has a significant amount of aerosols. Generally, the former provides the estimate of the surface contribution (e.g., surface reflectance), while the latter provides the estimate of aerosol amount (e.g., aerosol optical depth). One exception is the TOMS satellite, which senses aerosol absorption in the midtroposphere at ultraviolet wavelengths.

[4] Recently, satellite instruments have been launched which are designed to sense aerosol over land. These include the Along Track

[1]Visiting scientist at Office of Research and Applications, National Environmental Satellite, Data, and Information Service, National Oceanic and Atmospheric Administration, Camp Springs, Maryland, USA.

Copyright 2002 by the American Geophysical Union.
0148-0227/02/2001JD000505$09.00

Table 1. Aerosol Model Characteristics According to *Kaufman et al.* [1997] Where f_i is Normalized Such That $\sum f_i = 1$ in Calculations

Aerosol	Mode	r_m, μm	σ	f_i	ω_o
Continental	water-soluble	0.005	2.97	0.35	0.96
	dust-like	0.500	2.97	8×10^{-7}	0.96
	soot	0.0118	2.00	0.65	0.96
Biomass burning	accumulation	0.0448	1.82	0.999909	0.90
	coarse	0.982	3.52	0.000091	0.90
Urban	accumulation 1	0.036	1.82	0.895	0.96
	accumulation 2	0.114	1.57	0.105	0.96
	salt	0.990	1.35	2×10^{-4}	0.96
	coarse	0.670	2.56	3×10^{-7}	0.96
Dust	mode 1	0.001	2.12	0.987	0.92
	mode 2	0.0218	3.19	0.013	0.92
	mode 3	6.24	1.89	2×10^{-6}	0.92

Scanning Radiometer (ATSR-2) [*Veefkind et al.*, 1998], MODIS [*Kaufman et al.*, 1997; *Chu et al.*, 1998], MISR [*Diner et al.*, 1996], and Polarization and Directionality of Earth Reflectances (POLDER) [*Herman et al.*, 1997b]. These instruments use observations at multiple wavelengths or views in distinguishing the surface contribution from that of the aerosol. For example, the MODIS algorithm estimates surface reflectance over dense dark vegetation from the reflectance at 2.13 μm, where aerosol extinction is weak. This is related to the surface contribution at visible wavelengths, which then allows the retrieval of aerosol information. A more thorough review on aerosol retrieval algorithms over land and ocean is provided by *King et al.* [1999].

[5] The GOES aerosol optical depth (GOES-AOD) retrieval algorithm takes advantage of the fixed viewing geometries of a geostationary satellite and a recent sensor calibration by *Knapp and Vonder Haar* [2000] to retrieve aerosol optical depth. Using observations whose viewing geometry remains relatively constant

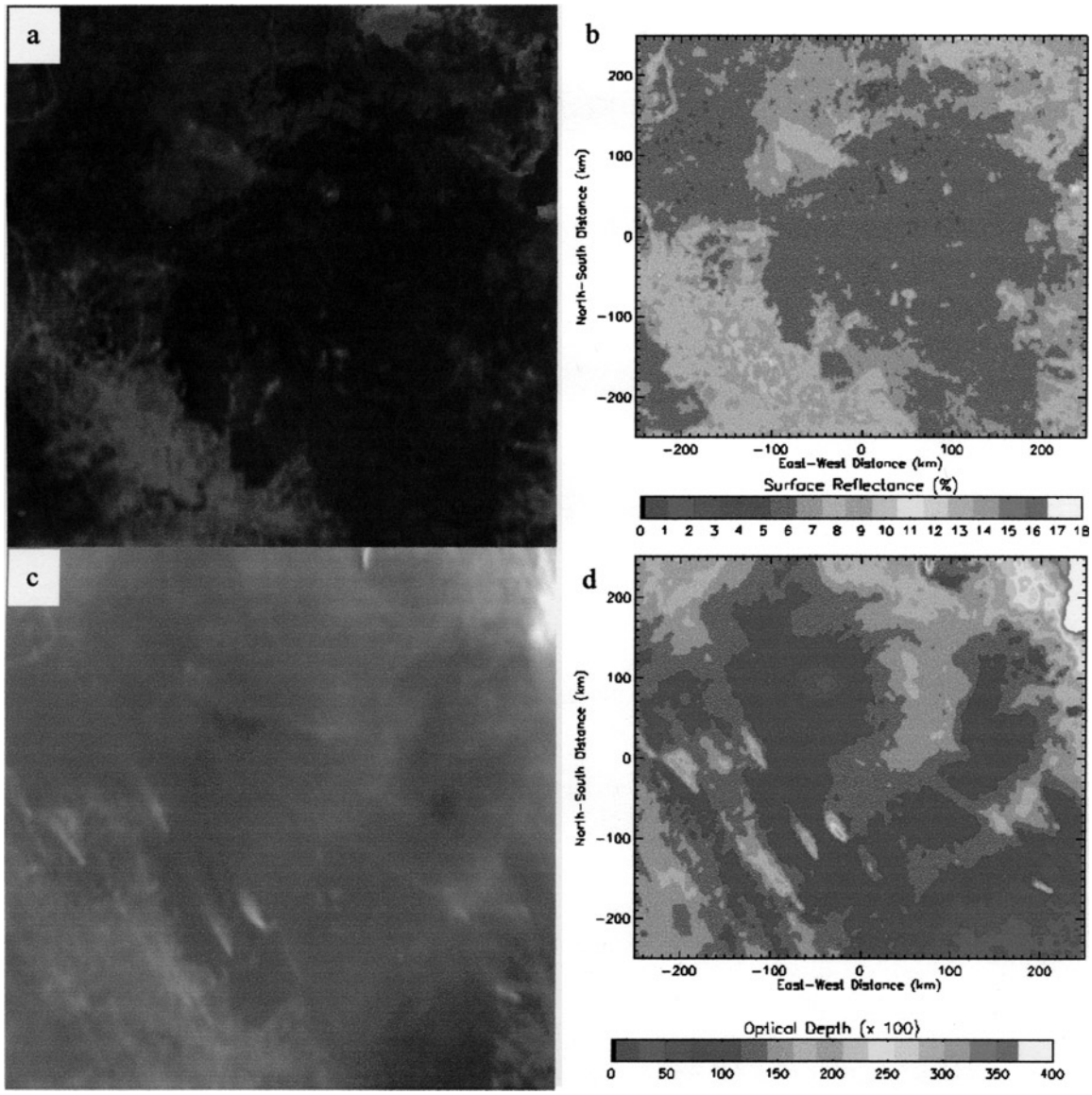

Figure 1. (a) 500 km × 500 km composite image over central Brazil during August 1998 for 1545 UTC. (b) *R* of the background image in Figure 1a where the reference point (0,0) is the Concepcion AERONET site. (c) GOES data from August 30, 1998, at 1545 UTC (same grayscale as Figure 1a) (d) GOES-AOD for image in Figure 1c using *R* in Figure 1b. See color version of this figure at back of this issue.

Table 2. Sources of Uncertainty in Retrieving Aerosol Optical Depth From Satellite

	Source
Atmospheric	aerosol optical properties (e.g., sphericity, ω_o, $n(r)$, refractive index)
	location of the aerosol layer
	Rayleigh optical depth
	gaseous absorption
Surface	reflectance uncertainty
	bidirectional reflectance contamination
Instrument	calibration
	noise
Radiative transfer model	plane-parallel approximation
	multiple scattering

decreases the dependence of top of the atmosphere (TOA) solar reflectances on the surface bidirectional reflectance. This is made possible by comparing satellite imagery from the same time of day, so day-to-day variation in Sun-Earth-satellite geometry is limited to only the daily solar declination angle variation. A background image is compiled by selecting the darkest observations of a location from time series of observations (one per day). This provides an estimate of the surface contribution through correction for atmospheric absorption and scattering. The aerosol contribution, aerosol optical depth, is then estimated by comparing imagery to the background composite image. The retrieval method is detailed in the next section followed by an analysis of the retrieval uncertainty. The algorithm is then validated against surface observations and compared to retrievals using airplane-based imagery.

2. GOES Aerosol Retrieval Method

[6] The GOES-AOD retrieval method uses the visible channel of the GOES-8 Imager instrument (0.52–0.72 μm FWHM) to retrieve aerosol information. This channel has a 1×1 km^2 resolution at nadir, and imagery is available at up to 15-min intervals (for more information on the GOES Imager, see *Menzel and Purdom* [1994]). The calibration coefficients from *Knapp and Vonder Haar* [2000] have been used to convert instrument counts to satellite-detected reflectance ρ_{sat} measurements.

2.1. Radiative Transfer Model

[7] The discrete ordinate radiative transfer (DISORT) model [*Stamnes et al.*, 1988] is used to stimulate ρ_{sat} observations. Radiative scattering and absorption in the atmosphere is simulated using six homogeneous and plane-parallel layers: two layers between the surface and 3 km and four layers above 3 km. Reflectances were calculated at eight wavelengths and integrated with GOES-8 visible spectral response to simulate ρ_{sat}. For each layer the optical depth, single scatter albedo ω_o, and scattering phase function are required; all atmospheric and aerosol properties are assumed in the retrieval except for aerosol optical depth. The atmospheric constituents which contribute to radiative scattering and absorption are Rayleigh scattering, gaseous absorption, and aerosol extinction. Primarily ozone and water vapor absorb at the wavelengths observed by the GOES-8 visible channel. The distribution of these gases was simulated following *McClatchey et al.,* [1971] for a tropical atmosphere (since the retrieval is validated in tropical South America), and gaseous absorption variations are ignored due to their small effect on ρ_{sat} [*Knapp and Vonder Haar*, 2000]. The surface is simulated by assuming a Lambertian surface reflectance R.

[8] The aerosol is simulated using a multimodal lognormal distribution following *Kaufman et al.* [1997] where four aerosol models are defined: continental, urban, biomass burning, and desert dust. While all four models are used in the following uncertainty analysis, only the biomass burning aerosol model is used in the retrievals because validations are in areas of biomass burning in South America. Each aerosol model size distribution $n(r)$ is simulated using

$$n(r) = \sum_{i=1}^{N} \frac{f_i}{r \ln \sigma_i} \exp\left[-\frac{\ln^2 r / r_{m,i}}{2 \ln^2 \sigma_i} \right],$$

where N is the number of modes per model, r is the radius, σ_i is the width of the mode, $r_{m,i}$ is the mode radius of mode i, and f_i is the number fraction of the total number for mode i. These parameters are provided in Table 1 for each aerosol model. The aerosol phase function is then calculated from $n(r)$ and the refractive index, $m = 1.4$, whose imaginary part produces the single scatter albedos provided in Table 1 using Mie scattering theory (which assumes spherical particles). Aerosol optical depth for aerosol layers above 3 km is fixed ($\tau = 0.025$), while τ below 3 km varies.

[9] The aerosol optical depth is retrieved using a look-up table (LUT). The radiative transfer model is used to calculate ρ_{sat} as a function of the geometric angles determined from the satellite viewing geometry and time of day, R, and τ (varied from 0. to 3.2). The retrieval then interpolates within the LUT, finding the τ which corresponds to the observed ρ_{sat} (and extrapolates when $\tau > 3.2$). The uncertainty in such a retrieval

Table 3. Parameters Randomly Varied in the Uncertainty Study

Parameter	Minimum	Maximum
τ	0.03	1.5
θ_o	1	50
θ	1	60
ϕ	0	180
R	0.0	0.12
τ_b	0.01	0.05
IAER[a]	1	4

[a] IAER represents the four aerosol models; it is an integer varying from 1 to 4.

Table 4. Standard Deviation σ of Gaussian Noise Added to the Retrieval Parameter in the Uncertainty Study for Cases A and B

	σ	
	Case A	Case B
ω_o	0.02	0.04
m	0.06	0.1
r_m	0.2 (20%)	0.3 (30%)
τ_b	0.02	0.04
ρ_{sat}	0.005	0.005
ρ_{min}	0.005	0.005
γ	0.022	0.022

Table 5. Summary of the Retrieval Uncertainty Study for Cases A and B

	Case A	Case B
R_e average	0.000	−0.001
σ_{Re}	0.003	0.003
Average τ_e	0.03	0.10
Median τ_e	0.00	0.00
σ_τ	0.27	0.69
ε	0.14	0.24

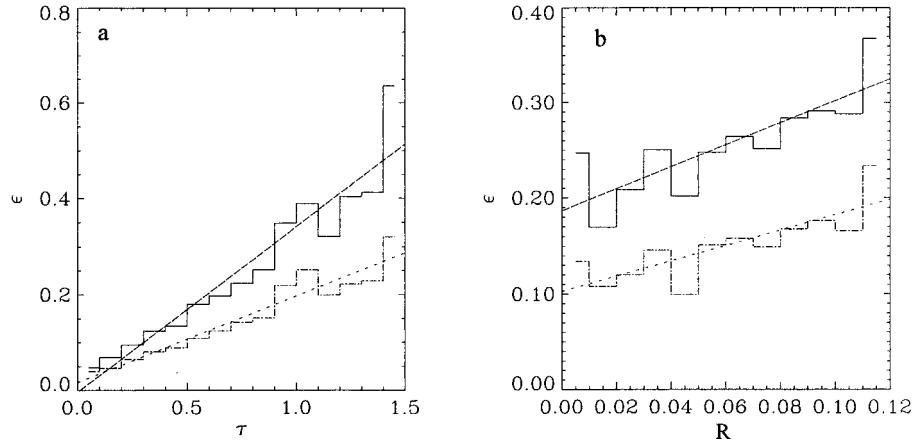

Figure 2. (a) Expected retrieval uncertainty ε versus τ for case A (dash-dotted line) and case B (solid line). The linear regression is $\varepsilon = 0.18\tau + 0.02$ ($r = 0.96$) for case A (dotted) and $\varepsilon = 0.34\tau + 0.0$ ($r = 0.95$) for case B (dashed). (b) Expected retrieval uncertainty ε versus R for case A (dash-dotted) with linear regression (dotted): $\varepsilon = 0.80\rho_s + 0.10$ ($r = 0.81$) and case B (solid line) with linear regression line (dashed): $\varepsilon = 1.16\rho_s + 0.19$ ($r = 0.81$).

is dependent upon the accuracy of the assumed model parameters and is discussed later.

2.2. GOES-AOD Algorithm

[10] The GOES-AOD algorithm incorporates a three-step process: compilation of the background composite, correction of atmospheric effects, and retrieval of aerosol optical depth. The validation is described in reference to retrievals made over South America in 1995 and 1998 when surface validation sites were measuring τ.

2.2.1. Compilation of the composite background. [11] The backbone of this approach is the creation of a background image from a time series of satellite images. A background image is created for each satellite observation time; during 1995 these occur over South America at 1145, 1445, and 1745 UTC and at 30-min intervals during 1998. Variations in the instrument attitude can cause significant errors in the location of surface features from image to image, so corrections were made manually to navigation parameters such that surface features showed little movement when looped. A simple reflectance threshold was used to mask for clouds and their shadows, which have a darker appearance than a normal scene and can contaminate the background image. Then the minimum (i.e., the darkest) GOES-8 visible satellite-detected reflectance ρ_{min} for a location is used in the background composite.

[12] An example of a composite background scene is presented in Figure 1a over Brazil during August 1998 (at 1545 UTC). A period of 2 months was used to create this background composite which provides 40–60 opportunities for a clear-sky observation of a pixel, similar to previous studies [*Jankowiak and Tanré*, 1992]. Uncertainty caused by temporal variation in the surface reflectance during these 2 months is discussed later. This clear-sky observation, however, is not completely free from atmospheric and aerosol extinction; these effects are removed using atmospheric correction.

2.2.2. Retrieval of surface reflectance. [13] The second step of the algorithm is the atmospheric correction (i.e., it removes atmospheric effects from the composite background). First, the satellite-detected counts (DC) are converted to ρ_{sat} via

$$\rho_{sat} = \frac{1}{\delta(D)\mu_o}\frac{DC - C_o}{\gamma},$$

where $\delta(D)$ is the correction for the Earth-Sun distance on day of year D, μ_o is the cosine of the solar zenith angle, C_o is the offset ($C_o = 29.2$), and γ is the calibration coefficient. For August 1995 and 1998, $\gamma = 806.3$ and 653.0, respectively [*Knapp and Vonder Haar*, 2000]. Atmospheric effects including gaseous absorption, molecular scattering, and aerosol extinction are removed via inversion of ρ_{min} to obtain an estimate of R. This step requires assumptions regarding the state of the atmosphere on the day ρ_{min} is observed. Again, the tropical atmosphere is used to estimate gaseous absorption and scattering. A background optical depth τ_b represents the remaining aerosol scattering in and is estimated from surface observations of τ from AERONET; where observations were not present, τ_b is assumed to be 0.05. The uncertainties of this assumption are discussed later. The surface retrieval for the background image in Figure 1a is shown in Figure 1b where values of R range from 5 to 10%.

2.2.3. Retrieval of aerosol optical depth. [14] The third step is the retrieval of τ, which attributes all variations of ρ_{sat} from ρ_{min} to changes in aerosol optical depth (in the absence of clouds and their shadows). As described above, the look-up table is interpolated for R, and then τ is retrieved by finding the reflectance in the table that matches ρ_{sat}. The retrieved τ is valid at 0.50 μm because this is the value used as input to the

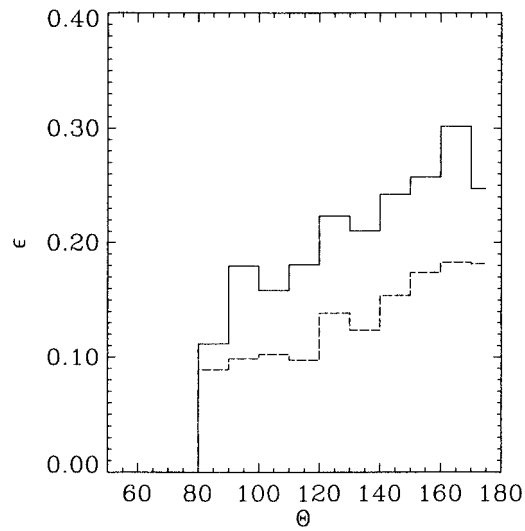

Figure 3. The parameter ε versus scattering angle Θ for case A (dashed line) and case B (solid line).

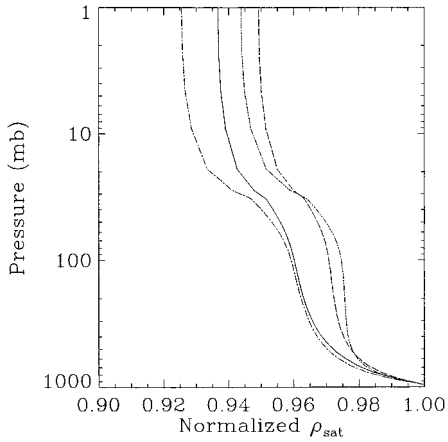

Figure 4. TOA ρ_{sat} for an aerosol layer at varying pressure levels normalized by ρ_{sat} from aerosol at 1000 mbar for $\tau = 0.3$ with $\omega_o = 1.0$ (dashed) and $\omega_o = 0.96$ (solid) and also $\tau = 1.0$ with $\omega_o = 1.0$ (dash-dot-dotted) and $\omega_o = 0.96$ (dash-dotted line).

radiative transfer model. A GOES image at 1545 UTC on August 30, 1998, is shown in Figure 1c (having the same grayscale as Figure 1a). The image is generally brighter with fire plumes present in the lower left; the corresponding GOES-AOD retrieval image is shown in Figure 1d where the smoke plumes have τ as high as 2.5.

3. Aerosol Retrieval Uncertainty Study

[15] The uncertainty in the retrieval of τ from satellite over land can be categorized as due to uncertainties in atmospheric properties, surface variations, instrument characteristics, and radiative transfer model errors. These uncertainties are summarized in Table 2. The atmospheric properties include gaseous constituents and Rayleigh optical depth as well as the location and properties of the aerosols themselves. The reflectance of the land surface is also uncertain because the magnitude (i.e., surface reflectance) and shape (i.e., bidirectional reflectance distribution function) of the surface is poorly characterized. Instrument noise and calibration errors lead to uncertainties in the detected radiance which can cause errors in retrieved R and τ. Finally, the radiative transfer (RT) model contains uncertainty in its ability to fully calculate the radiances at the range of angles observed. Most of these sources are investigated en masse in the following retrieval uncertainty simulation, and those which are difficult to include are investigated separately. The RT model uncertainty was not investigated herein since DISORT fully simulates multiple scattering and zenith angles (both solar and viewing) were well within the plane-parallel approximation.

3.1. Uncertainty for Random Conditions

[16] Numerous retrievals with random conditions are simulated in this analysis, using the collective results to estimate the retrieval uncertainty from numerous sources. First, random conditions are selected for solar zenith angle θ_o, view zenith angle θ, relative azimuth angle ϕ, aerosol model (IAER), τ, and R. The ranges of these parameters are provided in Table 3. These are used to simulate ρ_{sat} and ρ_{min}, via

$$\rho_{sat} = f(\theta_o,\ \theta,\ \phi;\ R;\ \tau,\ m,\ \omega_o,\ r_m,\ \text{IAER})$$

$$\rho_{min} = f(\theta_o,\ \theta,\ \phi;\ R;\ \tau_b,\ m,\ \omega_o,\ r_m,\ \text{IAER}),$$

where the function f is the DISORT model. The retrieval (f^{-1}) is simulated using DISORT-calculated look-up tables and the assumed model parameters with Gaussian-distributed noise (Δ) via

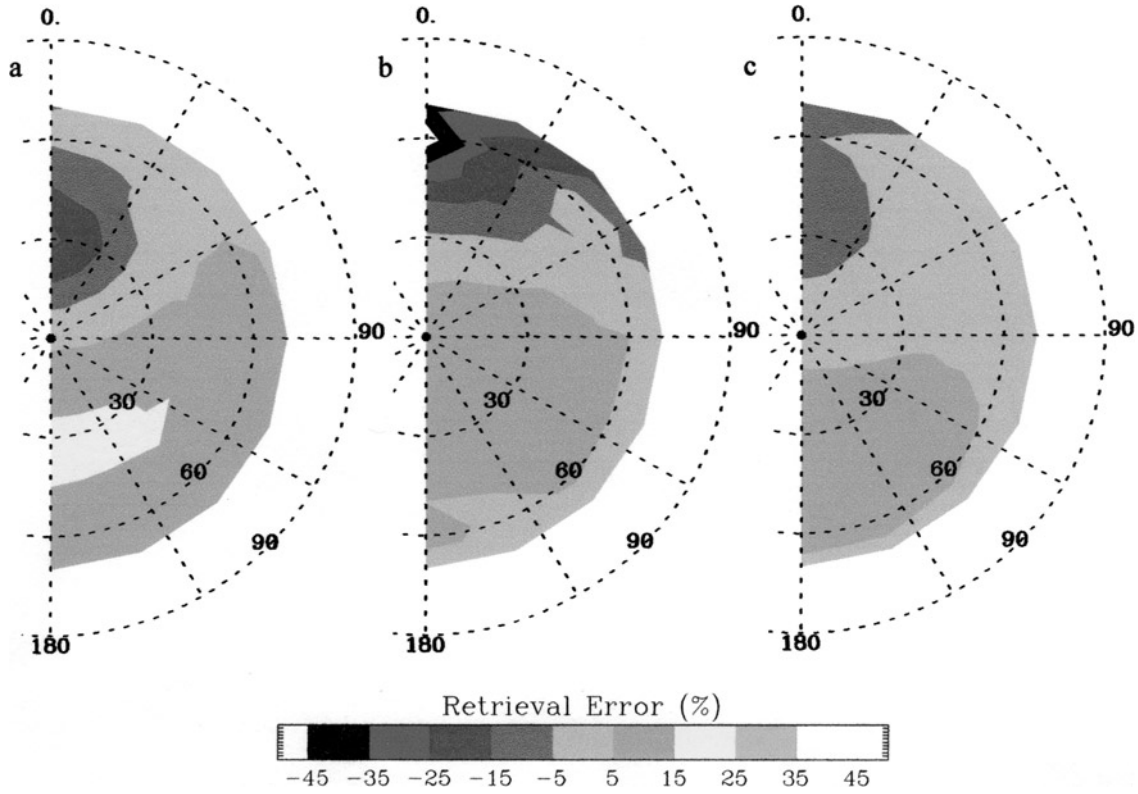

Figure 5. Retrieval error from assuming a Lambertian reflectance for a surface with a Rahman BRDF for (a) $\theta_o = 30$ and $\tau = 0.2$, (b) $\theta_o = 60$ and $\tau = 0.2$, and (c) $\theta_o = 30$ and $\tau = 1.5$. See color version of this figure at the of this issue.

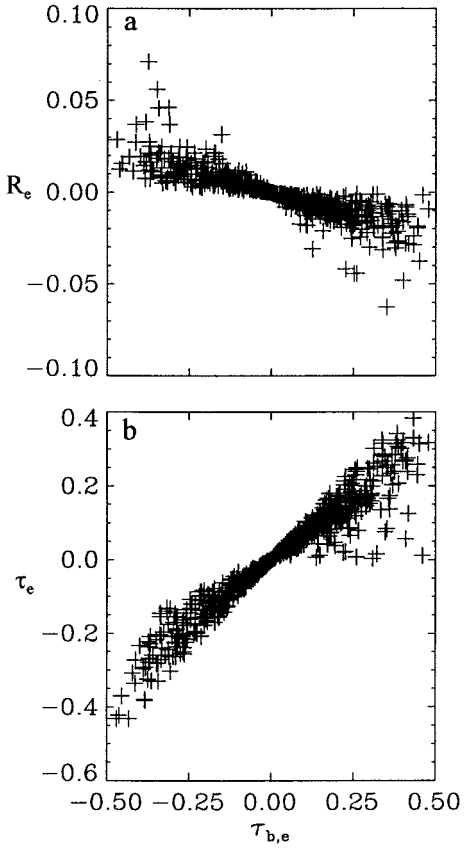

Figure 6. (a) Surface reflectance error as a function of background optical depth error and (b) aerosol optical depth error as a function of background optical depth error.

$$R_r = f^{-1}(\theta_o,\ \theta,\ \phi;\ \tau_b + \Delta\tau_b;\ \rho_{\text{sat}} + \Delta\rho_{\text{sat}},\ m + \Delta m,\ \omega_o + \Delta\omega_o,\ r_m + \Delta r_m,\ \text{IAER})$$

$$\tau_r = f^{-1}(\theta_o,\ \theta,\ \phi;\ R_r;\ \rho_{\text{sat}} + \Delta\rho_{\text{sat}},\ m + \Delta m,\ \omega_o + \Delta\omega_o,\ r_m + \Delta r_m,\ \text{IAER}).$$

The Gaussian-distributed noise assumes the model parameter error has no bias and has a standard deviation σ given in Table 4. Retrieval error in optical depth (τ_e) and surface reflectance (R_e) are then

$$R_e = R - R_r \qquad \tau_e = \tau - \tau_r.$$

The distributions of R_e and τ_e provide information on the dependence of the retrieval on assumed model parameters.

[17] This uncertainty study is then dependent on the range of conditions simulated and the size of the simulated noise. The parameters varied in the forward model, that is, the simulation of ρ_{sat} and ρ_{min}, are listed in Table 3 along with the range in which they were varied. The aerosol model is randomly selected to simulate uncertainty for all aerosol models. The magnitude of uncertainty is then estimated by simulating two ranges of model parameter uncertainty: case A, well known aerosol, and case B, unknown aerosol. So lower limits of aerosol uncertainty were chosen to represent a scenario where the aerosol is well-characterized. Conversely, the upper limit on uncertainty was chosen to simulate a retrieval of an aerosol layer with much less prior information on the aerosol optical properties. Therefore the lower and upper limits of retrieval uncertainty are (also in Table 4) as follows: $\sigma(\Delta\omega_o) = 0.02$ and 0.04, $\sigma(\Delta m_r) = 0.06$ and 0.1, $\sigma(\Delta r_m) =$ 20 and 30%, and $\sigma(\Delta\tau_b) = 0.02$ and 0.04. These ranges are chosen to bound the retrieval with an upper and lower limit of uncertainty. Satellite measurement uncertainty is simulated with $\sigma(\Delta\rho_{\text{sat}}) = \sigma(\Delta\rho_{\text{min}}) = 0.005$, which is equivalent to the averaging of a 5×5 array of pixels with a noise of 2.75 in digital counts, and the calibration uncertainty of 2% is rather conservative [*Knapp and Vonder Haar*, 2000]. The satellite values were constant for both cases since the primary area of concern is the effect of uncertainty in the aerosol optical properties. One thousand retrievals were simulated for each case.

[18] A summary of this uncertainty simulation is provided in Table 5. The simulated R_e shows no bias and has a standard deviation of 0.003. The simulated τ_r, however, has significant bias: 0.03 and 0.10 for cases A and B, respectively. The bias occurs because τ_e is rounded to zero when $\tau_r < 0$ causing a positive bias. Hence the median τ_e is zero. The standard deviations are quite large: 0.27 and 0.69 for cases A and B, respectively. The estimated error ε represents the 68th percentile of τ_e (i.e., the value of τ_e at which 68% of all $|\tau_e|$ fall below); for a normal distribution, $\varepsilon = \sigma$. It is used herein to represent the estimated retrieval error because (1) it is sensitive to the presence of retrieval outliers but not the magnitude of them and (2) it provides a smoother representation of error as a function of τ and R.

[19] The estimated error is a strong function of τ and R. The increase in ε with τ (Figure 2a) is 18 and 34% for cases A and B, respectively. A strong trend is also found in ε with respect to R (Figure 2b) where retrieval uncertainty increases with R. This is due to more contribution to ρ_{sat} from the surface than the aerosol and is consistent with *Kaufman* [1987]. Uncertainty also decreases as the scattering angle Θ decreases (Figure 3) where Θ is calculated from

$$\cos\Theta = \cos\theta_o\ \cos\theta + \sin\theta_o\ \sin\theta\ \cos\Delta\phi.$$

Less uncertainty occurs when zenith angles are large (i.e., when the path length through the atmosphere is larger) because the atmospheric contribution is larger. Overall, the expected retrieval uncertainty is ±34% and will likely be less in conditions when aerosol optical properties are better understood.

3.2. Other Sources of Uncertainty

[20] The simulation of random conditions does not allow simple estimation of all sources of uncertainty; specifically, those sources

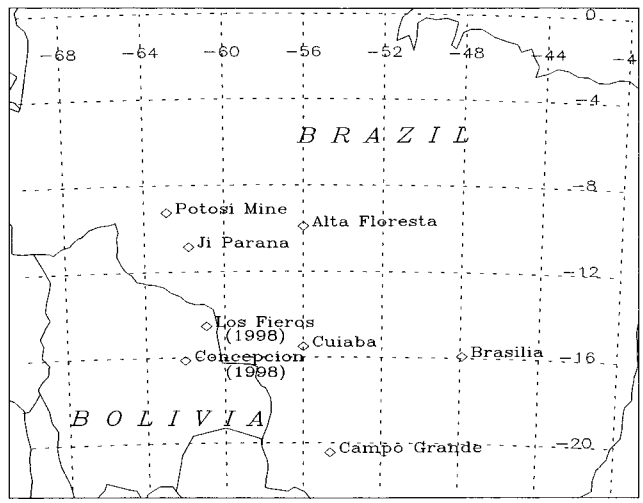

Figure 7. South American AERONET sites used for GOES-τ validation from 1995 and 1998.

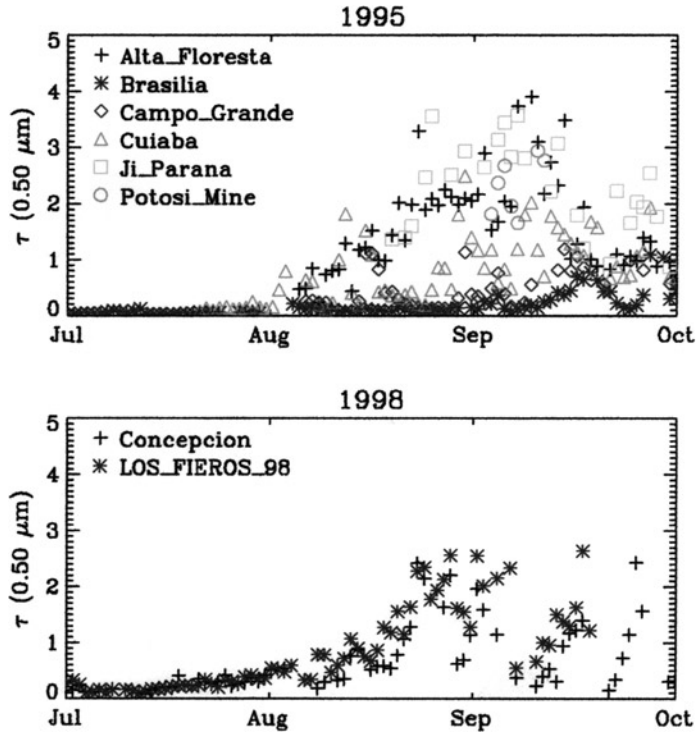

Figure 8. Time series of daily average aerosol optical depth (0.50 μm) at the AERONET sites used for GOES-AOD validation in 1995 and 1998. See color version of this figure at back of this issue.

which require the calculation of more look-up tables need to be examined in a different fashion. The following is a discussion of sources of uncertainties that were investigated separate from the study described above.

3.2.1. Uncertainty of the aerosol layer height. [21] The aerosol vertical distribution in the retrieval algorithm is adapted from the Moderate Resolution Transmittance (MODTRAN) RT model where the altitude of the maximum aerosol extinction is at the surface. However, aerosol layers are often located above the boundary layer. To simulate this uncertainty, the layer with the maximum τ has been varied to simulate an aerosol layer located somewhere between the surface and 100 mbar. The ratio of ρ_{sat} with the aerosol maximum at the surface to ρ_{sat} with the aerosol maximum at some pressure is then calculated (Figure 4). The solid line and dashed lines in Figure 4 show this ratio for an aerosol optical depth of 0.3 and 1.0, respectively, representing optically thin and thick aerosol layers at different altitudes. The change in ρ_{sat} is more pronounced with aerosol absorption (ω_o = 0.96) and less dependent upon aerosol optical depth. The retrieval is most sensitive to uncertainties near the surface where it is least sensitive to aerosol absorption. While it is difficult to quantify this uncertainty, an estimate of the maximum error expected can be made. The change in reflectance at 600 mbar (i.e., a 400 mbar error in the aerosol location) is 0.98 for $\omega_o = 1.0$ and 0.97 for $\omega_o = 0.96$. So, for a biomass burning aerosol ($\omega_o = 0.9$), the error could be as large as 0.95–0.96 in ρ_{sat}, which corresponds to a maximum error in τ of 0.15

3.2.2. Uncertainty of aerosol shape. [22] The calculations of aerosol scattering in the retrieval assume spherical particles, which may be inappropriate in some cases (e.g., desert dusts are generally nonspherical). *Mishchenko et al.* [1995] suggest that these errors can reach 100%, but in general, it is more pronounced for larger particles. Biomass burning particles are generally small, so the sensitivity to errors in sphericity will be more important for larger distributions, like desert dust. Nonetheless, biomass burning particles are well represented by spherical particles [*Martins et al.*, 1998], so this uncertainty is unlikely to affect the validation.

3.2.3. Uncertainty of the surface bidirectional reflectance. [23] Natural surfaces reflect radiation anisotropically, having a specific variation with illumination and viewing angles: the bidirectional reflectance distribution function (BRDF). Also, different surface types have different BRDFs, which can vary with the growth cycle of the surface cover. This can affect the τ retrieval through multiple scattering between the surface and the atmosphere. To understand the magnitude of this uncertainty, ρ_{sat} was simulated for a range of viewing geometries using the surface bidirectional reflectance distribution function of *Rahman et al.* [1993] and a fixed τ (where the surface parameters used are for a broadleaf forest [*Rahman et al.*, 1993]). These ρ_{sat} values are then used to retrieve τ assuming a Lambertian surface, which results in a different retrieved τ. The percent differences between the input and retrieved τ are presented in Figure 5 for three conditions: $\theta_o = 30^\circ$ with $\tau = 0.2$ (Figure 5a), $\theta_o = 60^\circ$ with $\tau = 0.2$ (Figure 5b), and $\theta_o = 30^\circ$ with $\tau = 1.5$ (Figure 5c). In general, the error is less than 15% except nearest the backscatter (where $\theta = \theta_o$ and $\Delta\phi = 180^\circ$, the surface "hot spot") where the errors approach −50%. Also, it is much less when τ is large because of less contribution from the surface relative to the aerosol. Therefore ignoring the BRDF could cause a small bias, usually less than 15% except in the backscatter region.

3.2.4. Uncertainty of the temporal surface variations. [24] The composite background (from the first step in the retrieval) is determined from a 2-month composite of visible imagery. This composite can be contaminated by surface reflectance variations during this time period. Possible sources of contamination include the seasonal growth cycle of vegetation or changes in reflectivity from rainfall (which occurs primarily in desert areas). Tropical rain forests, however, tend to have more uniform albedos through the year [*Csiszar and Gutman*, 1999] and are thus less susceptible to this error. Thus the retrieval uncertainty due to possible temporal changes in the surface will depend on the surface vegetation growing cycle and is likely small in the validation.

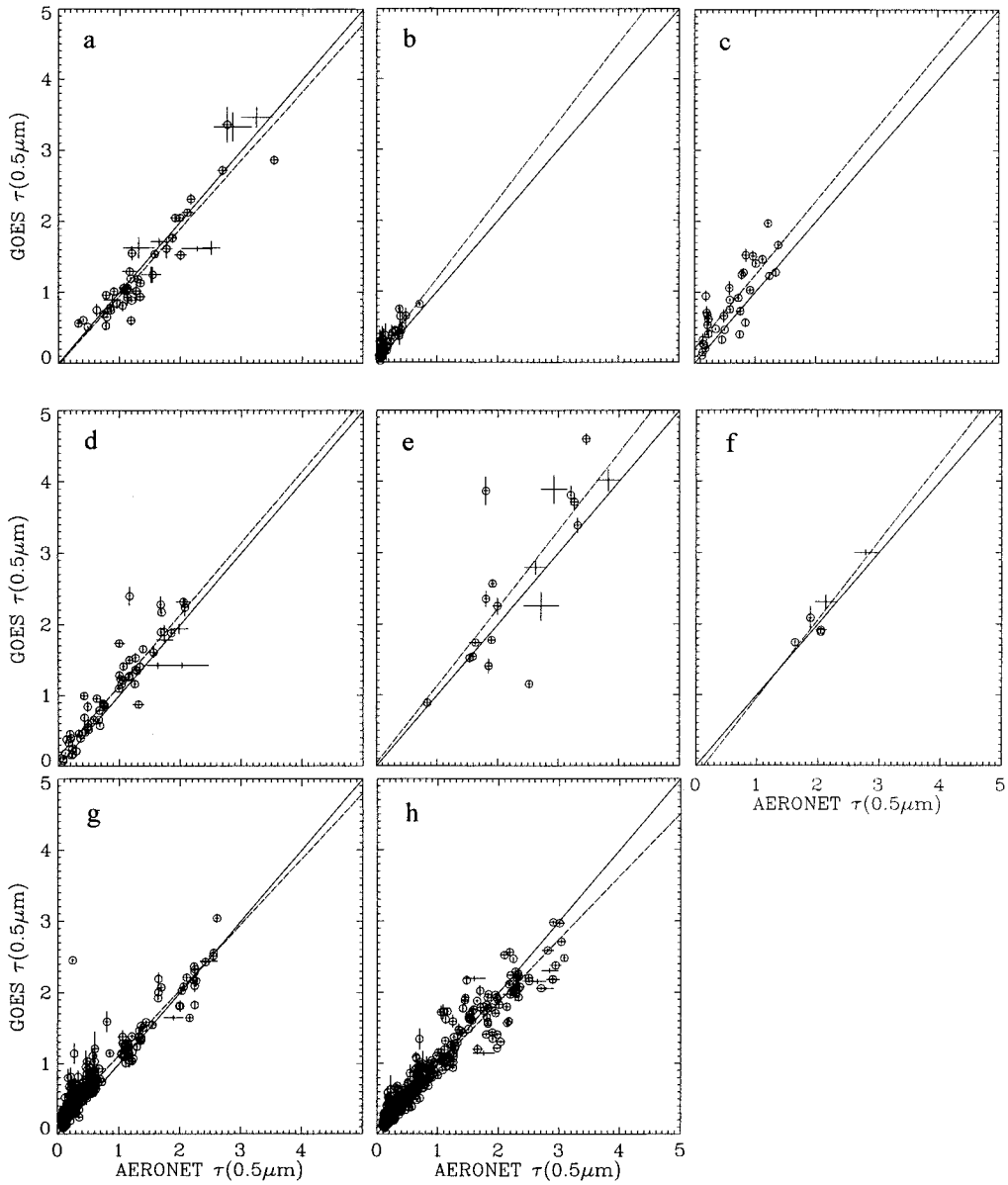

Figure 9. GOES τ versus AERONET τ (both at λ = 0.50 μm) for (a) Alta Floresta, (b) Brasillia, (c) Campo Grande, (d) Cuiaba, (e) Ji Parana, (f) Potosi Mine, (g) Concepcion, and (h) Los Fieros. The solid lines represent the one-to-one relationship, and dashed lines are the linear regression (statistics provided in Table 6) for each site. Horizontal bars represent temporal aerosol variations, vertical bars represent the spatial variation in the retrieved τ, and circles indicate where both variations are less than 0.2.

3.2.5. Uncertainty from gaseous absorption. [25] The primary gaseous absorbers in the spectral range of the visible channel of GOES-8 are water vapor and ozone which both have seasonal and temporal variations. However, the magnitude of these variations are small such that the effect on GOES-8 detected reflectance is generally undetectable. For example, the annual range of ozone over South America ranges from 240 to 310 Dobson units (as observed by TOMS). The corresponding range in visible optical depth is only 0.005. Water vapor absorption is similarly small. Again, for South America the range in integrated

Table 6. Statistical Values for the Validation of GOES τ With AERONET Including Number of Points *n*, Correlation Coefficient *r*, Linear Regression Slope and offset, bias σ_τ, and relative error $\sigma_\tau/\overline{\tau}$

Parameter	ALT	BRA	CAM	CUI	JIP	POT	CON	LOS
n	48	45	34	60	19	6	377	646
r	0.93	0.87	0.83	0.92	0.78	0.93	0.94	0.97
Slope	0.96	1.11	1.04	1.00	1.10	1.10	0.92	0.88
Offset	−0.02	0.08	0.20	0.13	0.04	−0.13	0.20	0.11
Bias	−0.07	0.10	0.23	0.14	0.25	0.07	0.16	0.04
σ_τ	0.29	0.09	0.27	0.25	0.71	0.17	0.18	0.17
$\sigma_\tau/\overline{\tau}$	0.20	0.52	0.45	0.27	0.31	0.08	0.38	0.28

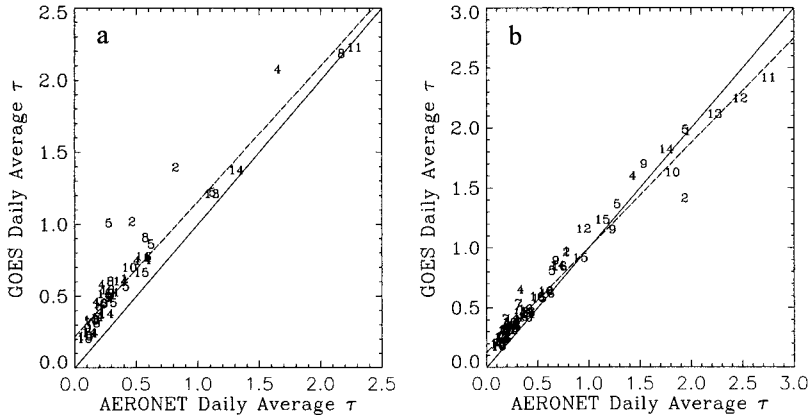

Figure 10. Daily average GOES τ versus AERONET τ (both at 0.50 μm) for (a) Concepcion and (b) Los Fieros (where plotted numbers represent the number of GOES observations used to estimate the daily average). Again, solid and dashed lines represent the one-to-one relationship and linear regression, respectively (linear regression statistics are provided in Table 7).

column water vapor (as estimated from AERONET observations) is from 2 to 6 g cm^{-2}, which has a corresponding variation of 0.007 in visible optical depth. So overall, the retrieval uncertainty resulting from uncertainty in column amounts of water vapor and ozone is less than 0.01.

3.2.6. Uncertainty in the assumed τ_b. [26] The length of time used in the composite method is a balance between using enough days to observe a clear sky and few enough days such that surface changes are minimized. In the event that a day with low aerosol burden is not observed, the assumed background optical depth τ_b will be wrong. To understand this problem, a separate error simulation using random conditions was performed where only the uncertainty in τ_b was varied, simulating errors up to 0.5. The resulting surface reflectance error is shown in Figure 6a as a function of the error in $\tau_b(\tau_{b,\,e})$. As τ_b is underestimated, less aerosol scattering is removed from the image leaving R too large; this propagates as an underestimate in the optical depth retrieval (Figure 6b). Most of the variation in retrieval error is explained by the τ_b error (correlation coefficient of 0.96), thus this effect is largely independent of solar geometry. The linear regression slope is 0.67 which suggests that the retrieval uncertainty is related by $\tau_e = 0.67\ \tau_{b,\,e}$. So an error in τ_b carries through to an error in τ_R, but it is not amplified; rather the retrieval error will be generally less than the retrieval by 67% of that error.

3.3. Summary of Retrieval Uncertainty

[27] As shown above, retrieval uncertainty can range from 18 to 34% depending upon the certainty of the aerosol optical properties, the instrument calibration, and the background optical depth. While conditions may exist to decrease this uncertainty (i.e., darker surfaces or larger zenith angles), conditions also exist which increase uncertainty, such as the presence of nonspherical particles or observations at the surface hot spot. Surface reflectance uncertainties, due to ignoring the surface BRDF and assuming a τ_b, can cause small biases in the retrieval which should be most noticeable when τ is small. Overall, the retrieval uncertainty is less than 40% and is optimally between 18 and 34%.

4. Retrieval Validation Over South America

4.1. SCAR-B Field Experiment

[28] The Smoke, Clouds, and Radiation—Brazil (SCAR-B) field experiment provided a thorough study of aerosols emitted from biomass burning in South America. In situ measurements allowed the characterization of numerous aerosol optical and physical properties [e.g., *Remer et al.*, 1998; *Yamasoe et al.*, 1998; *Reid and Hobbs*, 1998; *Martins et al.*, 1998] which provided more accurate optical properties of biomass burning aerosol. The Aerosol Robotic Network (AERONET) measured the aerosols at the surface (locations shown in Figure 7), while the MODIS airborne simulator (MAS) made observations at 20 km from a National Aeronautics and Space Administration (NASA) aircraft. This provides for validation of GOES-AOD with the AERONET as well as comparisons with MAS aerosol optical depth retrievals. Further results from SCAR-B are summarized by *Kaufman et al.* [1998].

4.2. Validation With Ground Truth

[29] The burn season in central South America generally begins in late July or early August and continues through October [*Prins et al.*, 1998]. During this time the aerosol optical depth increases as the smoke palls collect over Brazil, until transported south and eastward over the South Atlantic [*Trosnikov and Nobre*, 1998]. The time series of τ at the eight SCAR-B AERONET sites used for validation are shown in Figure 8. The sites nearer the burning, Ji Parana and Alta Floresta, have large optical depths with τ rarely less than 0.5 in August. Campo Grande, in a grassland region of southern Brazil, has lower optical depths. Cuiaba and Campo Grande have similar trends with large variability as smoke palls periodically advect over the sites. Also, Brasilia is included which is located far from the burn areas, thus aerosols there likely have different optical properties than the assumed biomass burning model. Yet it shows a significant aerosol optical depth increase in mid and late September. Two other sites, Concepcion and Los Fieros, were not present during the SCAR-B field study yet provide significant ground truth validation for 1998.

[30] Sun-sky radiometers provide excellent measurements of aerosol optical depth; however, there is still significant uncertainty when comparing to satellite observations. While the AERONET observations of τ have uncertainties of ±0.02 [*Holben et al.*, 1998],

Table 7. Same as Table 6, Except for Daily Average Validations at Concepcion and Los Fieros During 1998

Parameter	CON	LOS
n	46	55
r	0.96	0.98
Slope	0.87	0.94
Offset	0.13	0.22
Bias	0.19	0.04
σ_τ	0.14	0.14
$\sigma_\tau/\bar{\tau}$	0.27	0.20

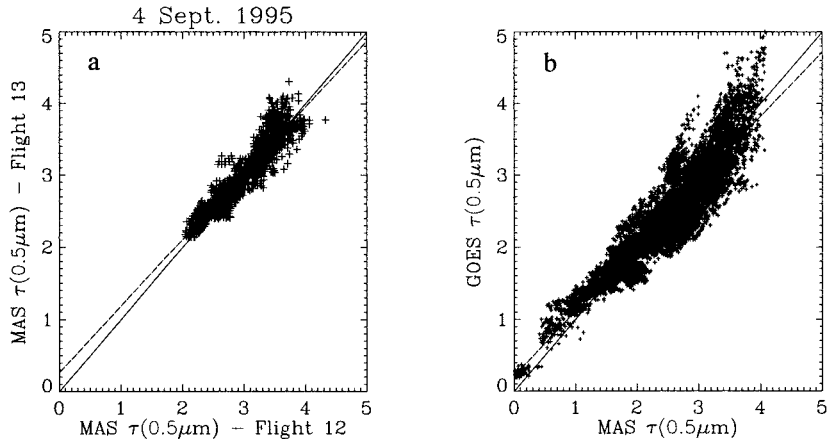

Figure 11. (a) Comparison of collocated MAS retrievals from September 4, 1995, for flight leg 12 versus 13 (measurements within ±30 min). (b) Comparison of GOES τ versus MAS τ for 15 flight legs for numerous MAS flights during SCAR-B (summary information provided in Table 9) for GOES imagery within ±30 min of the corresponding flight leg. Again, the solid and dashed lines represent the one-to-one relationship and linear regression, respectively (linear regression statistics are provided in Table 8).

larger uncertainties exist from differences in sampling volumes. The volume of air measured by the radiometer is a small cone from the sensor to the TOA, while the effective volume of the GOES-AOD is a combination of a 5×5 km^2 column (average of 5×5 pixels) extending from the surface toward the satellite as well as a similar column from the satellite footprint toward the Sun. Thus a radiometer observes a fraction of that sampled by the GOES-AOD, which requires a horizontally homogenous aerosol mass for consistent comparisons between the two. Therefore temporal averaging is applied to AERONET τ observations for ±30 min from the GOES-AOD. In an effort to reduce validation errors due to inhomogeneities, AERONET observations with large variations in τ during that time are removed from the validation.

[31] Calibrated and cloud-filtered AERONET observations were made at Alta Floresta (ALT), Brasilia (BRA), Campo Grande (CAM), Cuiaba (CUI), Ji Parana (JIP), and Potosi Mine (POT) for 1995 and Concepcion (CON) and Los Fieros (LOS) for 1998. The validations are plotted in Figure 9 by site with horizontal and vertical tick marks representing spatial (from GOES) and temporal (from AERONET) variations τ (points with circles denote points with both temporal and spatial variability less than 0.2). The linear regressions statistics of these validations are provided in Table 6. High correlation coefficients, r, are found at all eight AERONET sites, with r ranging from 0.78 to 0.97. Slopes of the linear regression lines show variation about 1 by 10%, perhaps caused by spatial variations in the aerosol optical properties. The positive bias at seven sites is within the expected noise and may be due to the assumption of the Lambertian surface (as described above). The standard error of regression (σ_τ) compared to the average observed optical depth ($\overline{\tau}$) ranges from 0.08 to 0.52; however, the larger relative errors are associated with lower $\overline{\tau}$; a more detailed analysis is provided by *Knapp* [2000]. The validation herein shows results within the ±18–34% range expected from the uncertainty study.

[32] The observations during 1998 provide an opportunity to compare daily averaged optical depths. The results of daily averaging are shown in Figure 10 where the numbers plotted represent the number of GOES observations used for the daily average; linear regression statistics are provided in Table 7. The correlation has increased, and the relative noise has significantly decreased from 0.38 and 0.28 to 0.27 and 0.20 (at Concepcion and Los Fieros, respectively). However, a slight positive bias is again apparent at lower optical depths, further suggesting an error in surface properties. Also, the aerosol optical properties could be quite different on days when the biomass burning is not a significant source; in these cases the absorption would be overestimated causing a positive bias at low optical depths. The outliers from the linear regression line are those days when fewer GOES observations were available, thus the daily aerosol optical depth was likely undersampled. So numerous observations from GOES provide a better estimate of aerosol optical depth.

4.3. Comparison With MODIS Airborne Simulator (MAS)

[33] The MODIS airborne simulator (MAS) flew more than a dozen flights during the SCAR-B experiment. The data from these flights have been processed by NASA to retrieve aerosol optical depth in a similar manner to the MODIS-Land algorithm. This provided an excellent test bed for the MODIS aerosol retrieval over land algorithm using MAS data (MAS-τ) which shows a strong correlation with Sun-sky radiometer observations during SCAR-B [*Chu et al.*, 1998]. The frequency of the MAS flights also allows an opportunity to intercompare the retrievals of aerosol from MAS-τ with the GOES τ retrievals. However, the frequency of MAS flights also allowed an intracomparison of the MAS-τ data.

[34] On September 4, 1995, the MAS instrument measured the same biomass burning plume twice, within 27 min when the NASA aircraft retraced its path. The aerosol optical depth retrievals for these flights, leg numbers 12 and 13, are collocated and compared in Figure 11a; the linear regression statistics are provided in Table 8. The differences in the comparisons are not necessarily errors with regard to the MAS-τ algorithm, but demonstrate the temporal variability of a smoke plume. Thus, when comparing GOES τ and MAS-τ, a portion of the variance ($\sim$0.18) can be explained by the difference in the observation time of each data set.

[35] There are 15 flight legs which are colocated with GOES τ retrievals (detailed in Table 9). In general, the flights are within

Table 8. Same as Table 6 Except for Comparisons of MAS–τ to MAS–τ and MAS–τ to GOES τ

Parameter	MAS-to-MAS	MAS-to-GOES
n	1,385	13,191
r	0.93	0.92
Slope	0.92	0.90
Offset	0.27	0.22
Bias	−0.032	0.019
σ_τ	0.18	0.27
$\sigma_\tau/\overline{\tau}$	0.060	0.11

Table 9. Summary of GOES τ Versus MAS$-\tau$ Comparisons With Observation Times of Each Retrieval[a]

Comparison	Day	MAS Flight Leg	GOES Image Time—Region, UTC	MAS Time, min	MAS$-\tau$ Range
1	Aug. 16	3	1501—BRA	−21 to −4	0.1–4.5
2	Aug. 23	10	1801—JIP	−32 to −19	2.5–4.0
3	Aug. 23	11	1801—JIP	−18 to −13	1.6–2.9
4	Aug. 23	12	1801—POT	−12 to +5	1.5–2.2
5	Aug. 23	12	1801—JIP	−12 to +5	1.4–2.2
6	Aug. 30	2	1501—CUI	−10 to +12	2.4–4.0
7	Sept. 1	8	1501—CUI	−32 to −13	0.5–2.3
8	Sept. 1	11	1501—CUI	+3 to +28	0.5–2.6
9	Sept. 4	1	1501—CUI	−18 to +5	0.4–1.1
10	Sept. 4	12	1801—POT	−30 to −19	1.9–4.1
11	Sept. 4	13	1801—POT	−11 to −3	2.1–4.1
12	Sept. 4	15	1801—POT	+3 to +24	2.0–3.7
13	Sept. 7	1	1501—CUI	−8 to +10	0.5–2.1
14	Sept. 7	12	1801—JIP	−30 to −4	2.0–4.1
15	Sept. 7	12	1801—POT	−30 to −4	2.0–3.9

[a] MAS observation time is relative to the GOES image time.

±30 min of the GOES image observation. These colocations occur near various AERONET sites (and thus over a variety of surface types), have differences in time as large as 32 min, and numerous ranges in τ. The comparison of all MAS-τ with GOES τ is provided in Figure 11b (with linear regression statistics in Table 8). The correlation is very high, with statistics similar to the MAS-τ intracomparison. The noise is only slightly higher (σ_τ = 0.27), and relative to $\bar{\tau}$ the error is only 11%. There does seem to be a nonlinear trend when MAS-τ is greater than 2, which is likely caused by differences in the retrieval algorithms. Nonetheless, the agreement between the two methods is significant and suggests the possibility of using GOES aerosol retrievals to augment the low-temporal resolution MODIS τ retrievals.

5. Conclusions

[36] A method for deriving aerosol information from GOES-8 imagery is described and validated over South America. The retrieval algorithm creates a composite image by selecting the darkest pixels from a time series of reflectances, where angular reflectance effects are minimized by using imagery from the same time of day. The surface reflectance is estimated from this composite by removing gaseous absorption, Rayleigh scattering, and aerosol extinction. Aerosol optical depth is then retrieved using the retrieved surface reflectance and GOES imagery. The uncertainty study suggests errors range from 18 to 34% depending on the accuracy of the assumed model parameters. Larger retrieval errors can occur from incorrect assumptions of aerosol optical properties (especially in the presence of aspherical particles), aerosol layer height, or for observations near the backscatter angle. While persistent haze represents a difficulty with this method, future MODIS retrievals could be used to resolve the ambiguity of the background aerosol optical depth. Also, retrieval uncertainty was found to be less over darker surfaces and at larger zenith angles.

[37] The retrieval algorithm was applied to GOES imagery of South America for July through September of 1995 and 1998. During this time, biomass burning aerosol is frequently observed. Comparison with Sun-sky radiometer showed significant correlations, ranging from r = 0.78 to 0.97. Retrieval errors were less than 38% at all but two sites. Also, daily averages of the retrieved optical depths showed less noise and higher correlations than the instantaneous validations.

[38] The GOES-AOD algorithm compared well with the MAS-AOD retrievals, as shown by the comparison with MAS flight data. Comparisons are well within the limits described by the uncertainty study and thus show that aerosol information can be estimated from GOES-8. The MODIS algorithm represents the state-of-the-art in aerosol remote sensing, whereas the GOES-AOD algorithm represents the ability of previous sensors. Thus information from the two algorithms is quite comparable and can be combined to provide a high temporal resolution data set to observe the changes of the biomass burning as well as other sources visible from GOES-8.

[39] **Acknowledgments.** Many thanks to Brent Holben and NASA for providing AERONET data, Rong-Rong Li for providing the MAS aerosol optical depth measurements, and committee members Mahmood Azimi-Sadjadi, Yoram Kaufman, Sonia Kreidenweis, and Graeme Stephens for their review of this research. This research was supported by Department of Defense Center for Geosciences/Atmospheric Research agreement DAAL01-98-2-0078 and the Center for Earth and Atmosphere Studies (CEAS under NASA contract NCC5-288).

References

Chu, D. A., Y. J. Kaufman, L. A. Remer, and B. N. Holben, Remote sensing of smoke from MODIS airborne simulator during the SCAR-B experiment, *J. Geophys. Res.*, *103*, 31,979–31,988, 1998.

Csiszar, I., and G. Gutman, Mapping global land surface albedo from NOAA AVHRR, *J. Geophys. Res.*, *104*, 6215–6228, 1999.

Diner, D. J., et al., Multi-angle Imaging Spectro-Radiometer: Level 2 Aerosol retrieval algorithm, *EOS ATBD-JPL D-11400, Rev. B*, 81 pp., 1996.

Fraser, R. S., Y. J. Kaufman, and R. L. Mahoney, Satellite measurements of aerosol mass transport, *Atmos. Environ.*, *18*, 2577–2584, 1984.

Hansen, J., M. Sato, R. Ruedy, A. Lacis, and V. Oinas, Global warming in the twenty-first century: An alternative scenario, *Proc. Natl. Acad. Sci. U.S.A.*, *97*, 9875–9880, 2000.

Herman, J. R., P. K. Bhartia, O. Torres, C. Hsu, C. Seftor, and E. Celarier, Global distributions of UV-absorbing aerosols from Nimbus-7/TOMS data, *J. Geophys. Res.*, *102*, 16,911–16,922, 1997a.

Herman, M., J. L. Deuzé, C. Devaux, P. Goloub, F. M. Bréon, and D. A. Tanré, Remote sensing of aerosols over land surfaces inducing polarization measurements and application to POLDER measurements, *J. Geophys. Res.*, *102*, 17,039–17,050, 1997b.

Holben, B. N., et al., AERONET—A federated instrument network and data archive for aerosol characteristics, *Remote Sens. Environ.*, *66*, 1–16, 1998.

Jankowiak, I., and D. Tanré, Satellite climatology of Saharan dust outbreaks: Method and preliminary results, *J. Clim.*, *5*, 646–656, 1992.

Kahn, R., R. West, D. McDonald, B. Rheingans, and M. I. Mishchenko, Sensitivity of multiangle remote sensing observations to aerosol sphericity, *J. Geophys. Res.*, *102*, 16,816–16,870, 1997.

Kaufman, Y. J., Satellite Sensing of aerosol absorption, *J. Geophys. Res.*, *92*, 4307–4317, 1987.

Kaufman, Y. J., R. S. Fraser, and R. A. Ferrare, Satellite remote sensing of large-scale air pollution: Method, *J. Geophys. Res.*, *95*, 9895–9909, 1990.

Kaufman, Y. J., D. Tanré, L. A. Remer, E. F. Vermote, A. Chu, and B. N. Holben, Operational remote sensing of tropospheric aerosol over land

from EOS moderate resolution imaging spectro-radiometer, *J. Geophys. Res.*, *102*, 17,051–17,068, 1997.

Kaufman, Y. J., et al., Smoke, Clouds, and Radiation-Brazil (SCAR-B) experiment, *J. Geophys. Res.*, *103*, 31,783–31,805, 1998.

Kaufman, Y., B. N. Holben, D. Tanré, I. Slutsker, A. Smirnov, and T. F. Eck, Will aerosol measurements from Terra and Aqua polar orbiting satellites represent the daily aerosol abundance and properties?, *Geophys. Res. Lett.*, *27*, 3861–3864, 2000.

King, M. D., Y. J. Kaufman, D. Tanré, and T. Nakajima, Remote sensing of tropospheric aerosol from space: Past, present and future, *Bull. Am. Meteorol. Soc.*, *80*, 2229–2259, 1999.

Knapp, K. R., Aerosol retrieval over land using background composites of geostationary satellite data, Ph.D. thesis, Colo. State Univ., Fort Collins, 2000.

Knapp, K. R., and T. H. Vonder Haar, Calibration of the eighth geostationary observational environmental satellite (GOES-8) Imager visible sensor, *J. Atmos. Oceanic Technol.*, *17*, 1639–1644, 2000.

Lyons, W. A., J. C. Dooley Jr., and K. T. Whitby, Satellite detection of long-range pollution transport and sulfate aerosol hazes, *Atmos. Environ.*, *12*, 621–631, 1978.

Martins, J. V., P. V. Hobbs, R. E. Weiss, and P. Artaxo, Sphericity and morphology of smoke particles from biomass burning in Brazil, *J. Geophys. Res.*, *103*, 32,051–32,058, 1998.

McClatchey, R. A., R. W. Fenn, J. E. A. Selby, F. E. Volz, and J. S. Garing, Optical properties of the atmosphere, *AFCRL-TR-71-0279*, *Environ. Res. Pap.354*, L. G. Hanscom Field, Bedford, Mass., 1971.

Mekler, Y., and Y. J. Kaufman, The effect of Earth's atmosphere on contrast reduction for a nonuniform surface albedo and the "two-halves" field, *J. Geophys. Res.*, *85*, 4067–4083, 1980.

Menzel, W. P., and J. F. W. Purdom, Introducing GOES-I: The first of a new generation of Geostationary Operational Environmental Satellites, *Bull. Am. Meteorol. Soc.*, *75*, 757–781, 1994.

Mishchenko, M. I., A. A. Lacis, B. E. Carlson, and L. D. Travis, Nonsphericity of dust-like tropospheric aerosols: Implications for aerosol remote sensing and climate modeling, *Geophys. Res. Lett.*, *22*, 1077–1080, 1995.

Mishchenko, M. I., L. D. Travis, and D. W. Mackowski, T-matrix computations of light scattering by nonspherical particles: A review, *J. Quant. Spectrosc. Radiat. Transfer*, *55*, 535–575, 1996.

Prins, E. M., J. M. Fetz, W. P. Menzel, and D. E. Ward, An overview of GOES-8 diurnal fire and smoke results for SCAR-B and 1995 fire season in South America, *J. Geophys. Res.*, *103*, 31,821–31,835, 1998.

Rahman, H., B. Pinty, and M. M. Verstraete, Coupled surface atmosphere reflectance (CSAR) model, 2, Semiempirical surface model usable with NOAA advanced very high resolution radiometer data, *J. Geophys. Res.*, *98*, 20,791–20,801, 1993.

Reid, J. S., and P. V. Hobbs, Physical and optical properties of young smoke from individual biomass fires in Brazil, *J. Geophys. Res.*, *103*, 32,013–32,030, 1998.

Remer, L. A., Y. J. Kaufman, B. N. Holben, A. M. Thompson, and D. McNamara, Biomass burning aerosol size distribution and modeled optical properties, *J. Geophys. Res.*, *103*, 31,879–31,891, 1998.

Soufflet, V., D. Tanré, A. Royer, and N. T. O'Neill, Remote sensing of aerosols over Boreal forest and lake water from AVHRR data, *Remote Sens. Environ.*, *60*, 22–34, 1997.

Stamnes, K., S. C. Tsay, W. Wiscombe, and K. Jayaweera, Numerically stable algorithm for discrete-ordinate-method radiative transfer in multiple scattering and emitting layered media, *Appl. Opt.*, *27*, 2502–2509, 1988.

Tanré, D., Y. J. Kaufman, M. Herman, and S. Mattoo, Remote sensing of aerosol properties over oceans using the MODIS/EOS spectral radiances, *J. Geophys. Res.*, *102*, 16,971–16,988, 1997.

Trosnikov, I. V., and C. A. Nobre, Estimation of aerosol transport from biomass burning areas during the SCAR-B experiment, *J. Geophys. Res.*, *103*, 32,129–32,138, 1998.

Veefkind, J. P., G. de Leeuw, and P. A. Durkee, Retrieval of aerosol optical depth over land using two-angle satellite radiometry during TARFOX, *Geophys. Res. Lett.*, *25*, 3135–3138, 1998.

Yamasoe, M. A., Y. J. Kaufman, O. Dubovik, L. A. Remer, B. N. Holben, and P. Artaxo, Retrieval of the real part of reflectance index of smoke particles from Sun/sky measurements during SCAR-B, *J. Geophys. Res.*, *103*, 31,893–31,902, 1998.

Y. J. Kaufman, NASA Goddard Space Flight Center, Greenbelt, MD 20771, USA.

K. R. Knapp, Office of Research and Applications, National Environmental Satellite, Data, and Information Service, NOAA, 5200 Auth Road, Room 711, Camp Springs, MD 20746-4304, USA. (ken.knapp@noaa.gov)

T. H. Vonder Haar, Cooperative Institute for Research in the Atmosphere and Department of Atmosphere Science, Colorado State University, Fort Collins, CO 80521, USA.

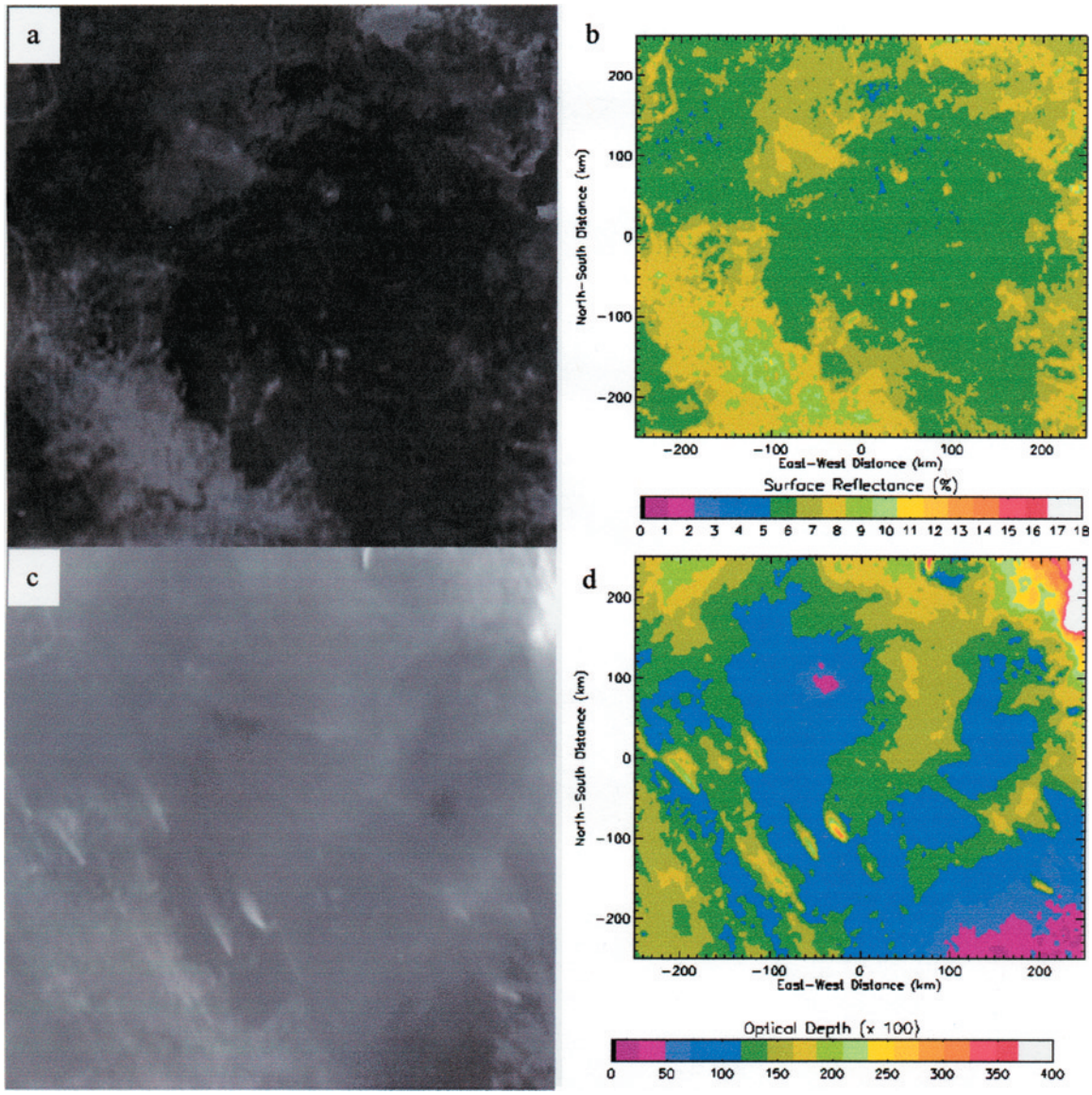

Figure 1. (a) 500 km × 500 km composite image over central Brazil during August 1998 for 1545 UTC. (b) *R* of the background image in Figure 1a where the reference point (0,0) is the Concepcion AERONET site. (c) GOES data from August 30, 1998, at 1545 UTC (same grayscale as Figure 1a) (d) GOES-AOD for image in Figure 1c using *R* in Figure 1b.

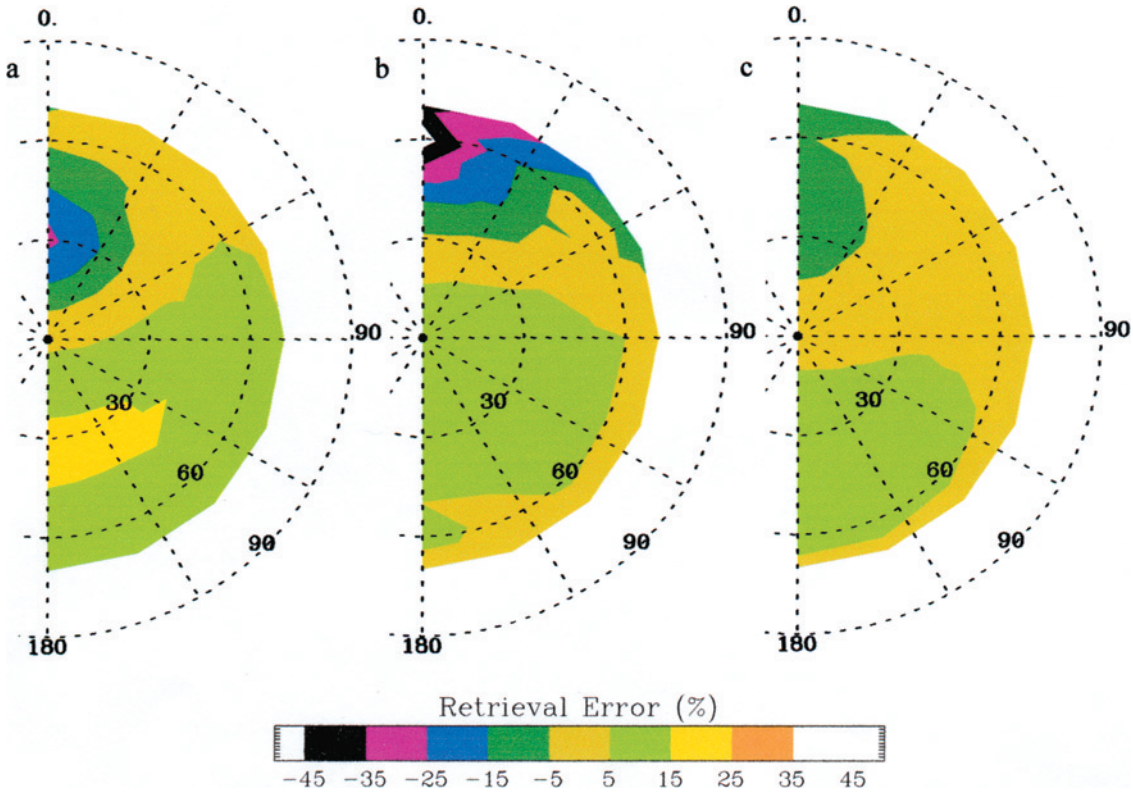

Figure 5. Retrieval error from assuming a Lambertian reflectance for a surface with a Rahman BRDF for (a) $\theta_o = 30$ and $\tau = 0.2$, (b) $\theta_o = 60$ and $\tau = 0.2$, and (c) $\theta_o = 30$ and $\tau = 1.5$.

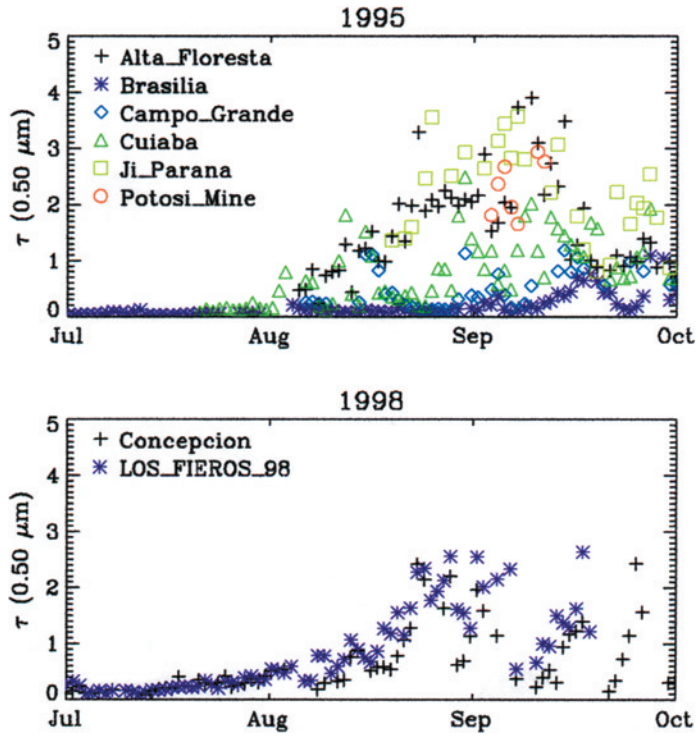

Figure 8. Time series of daily average aerosol optical depth (0.50 μm) at the AERONET sites used for GOES-AOD validation in 1995 and 1998.